Effect of grain size and shape on undrained behaviour of sands

Soheil Ghadr[1*], Arya Assadi-Langroudi[2]

[1*] [Corresponding Author] PhD, Civil engineering department, Urmia University, Oroumieh, Iran
   Tel: +98914 340 9081
   Email: s.ghadr@urmia.ac.ir

[2] Senior Lecturer in Geotechnical Engineering, University of East London, London, E16 2RD, England
   Email: A.AssadiLangroudi@uel.ac.uk

Abstract:

The stress-strain and stress path characteristics of sands are influenced by their grain size, shape, and packing. Morphological characteristics and size of particles play important role on the undrained shear strength of sands. Often, effects of these parameters are complex and cannot be easily distinguished. This study advances the knowledge of the role of particle size and shape on the undrained shear strength of sands. To eliminate the consequence of morphological characteristics, two sands with different particle sizes but similar angularity, and another sand with different roundness were selected for the study. These morphological characteristics for all three sands were determined from the analysis of scanning electron microscope images. F131 sand with higher median grain size and lower shape factors (r_r and r_s) had highest undrained peak shear strength and phase transformation value. Undrained strength (q_{pt}) and effective principal stress ($P'pt$) in phase transformation point had direct relationship with grain median grain size (D_{50}) and inversely effect of shape factor (r_r and r_s). F131 and F161 sands represented highest peak and ultimate steady state strengths, respectively. Flow potential appeared to be directly proportional with (r_r and r_s) and inversely with D_{50}. The peak index decreased with increasing shape factors (r_r and r_s).

Key words: Particle size; Morphology; undrained shear strength; flow potential; flow potential

Introduction

Study of the effects of particle shape and size distribution on the behaviour of soils improves the application and understanding of laboratory test results [1, 2]. Characteristics such as particle shape and size combinations have been investigated by many researchers since the 1950s, nonetheless the significance of particle size ratios in mechanics of sand-gravel, sand-silt and sand-clay granular mixtures has remained a subject of dispute [3 -7]: Holtz and Gibbs [3] presented results of triaxial tests on mixtures of gravel and sand in different proportions and reported that the shear strength increase as gravel content reaches levels higher than 50–60 % (by weight). Simoni and Houlsby [8] showed that even at low gravel contents (10–20 %) in sand-gravel mixture, gravelly sands packed to the same density of pure sand exhibit higher constant volume strength, maximum dilatancy rate, and peak strength. The scale-dependent porosity of composite geomaterials has confused the understanding of undrained behaviour of binary sand-silt mixtures. For sand-clay mixtures, Vallejo and Zhou [5] reported improved shear strength when the sand content is less than 50 % in the clay matrix and when the sand content is more than 80 % in the sand fraction. Ghadr and Assadi-Langroudi [10] adopted a micromechanical approach to show, for a constant void ratio, any variation in clay content in sand-clay systems rebalances the macro-to micro-pores volume ratio and the alteration in the packing state is controlled by sand particles shape and sorting. They continued to demonstrate the negligible control on compression index of sand particles shape/grading in systems with low clay content (i.e Small Clay) and attributed it to the implications of particles' interlocking and the peculiar distribution of clay platelets at low contents across sandy matrix. This is an unusual observation when compared with soil behaviour in sand-silt mixtures. Ghadr and Assadi-Langroudi [10] concluded that whilst grain asperities enhance the strength of the composite materials, higher angularity also leads to greater degrees of swelling potential/pressure, volumetric, axial, and diametric shrinkage strains on moving from 'Small Clay' to 'Large Clay'. This highlights the interacting

2

particle shape and size in defining the complex reliance of soil behaviour on sand geometrical characteristics.

For pure sandy soils and at sand assemblage level, association of mechanical properties with sand size (and shape) has received relatively little attention. Tsomokos and Georgiannou [11] showed substantial changes to response of sands with similar grading and varied shape. Oda et al. [12] presented fresh experimental evidences in support of the role particle alignment plays in controlling mechanical characteristics of sand. They showed that sand particles preferred alignment (upon re-arrangement, for example due to water inflow or overburden) decreases as particle roundness decrease (towards rod or flat shape). In other words, sand grains of non-symmetrical shape are more likely to retain their original random orientation which will logically yield greater orders of interlocking, friction and shear strength. Seminal works include contributions of several researchers [13-14, 7]. Cho et al. [7] showed that enhanced angularity generally yields packings of greater porosity. They defined a 'particle regularity' index parameter, as the average of sphericity and roundness measured through formulations offered in [15], and demonstrated that particle irregularity is directly proportional with confined compressibility (i.e. Oedometric compression index), critical state friction angle and intercept Γ of the critical state line. Decrease in either of sphericity and/or roundness (increased angularity or plainness) would increase the dilative response and hence peak friction angle (depending on particle alignment in relation to the shear direction) and decrease the small strain stiffness [16-19]. Shear strength in frictional (cohesionless) materials gains value as the angular solids form over 20% by mass of the assemblage [20-21], although some workers restricted this relevance to isotropic sands only [22]. For anisotropic loading environments, Tsomokos and Georgiannou [11] presented findings from a series of undrained monotonic torsional hollow cylinder triaxial tests on four fine to medium uniform sands. For test sands packed to similar relative density (before shearing) and nearly identical particle size distribution, rounded particle shape yielded strain softening and flow as compared with sub-angular particle shape that led to dilative

response (depending on density) with increasing torsional load. The observed association of peak strength and post-peak stress-strain response with shape continued to be valid in undrained compression triaixial test data. The relevance of particles orientation (packing state), shape and size, on soil mechanical behaviour is complex; the experimental datasets are small and the subject is still of extensive interest. These complex associations appear at grain scale and have received some previous attention:

Whether or not a universal sand breakage mechanism that is independent from the quality and crystalline intactness of detrital parent rock exists is still disputed; this adds to the complexities of relevance of particles orientation (packing state), shape, texture and size on strength of granular assemblages. This paper tends to further the knowledge through a limited 12 number of undrained compression triaxial shear tests on three sands, carefully chosen to allow the study of shape, size and crystalline integrity independently.

Static Flow and Steady States in Sand

Static loading has a significant role in the commencement of liquefaction as well as the post-liquefaction flow slides [23-25]. The static shear stress in the soil can be the driving force of flow slides, after the initiation of liquefaction [25-26]. Sand typically shows dilative volume changes at low confining pressure levels and as deviator stress levels approach failure. This stress-dependent transition, from an initial compressive to dilative behaviour, takes place along a 'phase transformation' (PT) line under undrained conditions on the stress space. The location of the phase transformation line is dependent on minor and intermediate principal stresses and on the relative density of sand [27]. On the q-p' space, phase transformation occurs on the effective stress path and where the stress path changes in direction i.e. axis point of curvature, where the effective mean normal stress (p') reaches a minimum value (Fig. 1a). Taking 'steady state' as the state of deformation under constant stress components [28-30], the point of phase transformation can be regarded as a 'steady state'. This state is broadly referred to as the quasi-steady

state (QSS), where post-peak deformations appear under constant effective mean stress p'. The QSS is followed by the ultimate steady state (USS). Unlike dense sands, in loose sands under low confinement levels, at the point of phase transformation, the QSS occurs at minimum shear stress (Fig. 1b - also see [31]). A course of strain hardening will normally follow the QSS unless sand is at reasonably large levels of initial effective confining pressures (or is at a very loose state whereby confining pressure turns out to be relatively large). In this case, no post-peak hardening develops, and the minimum stress state evolves into the critical steady state (CSS).

Materials and Methods

Uniformly-graded well-sorted Firoozkuh 161 (F161) and 131 (F131) silica sands (sub-angular) and Urmia Lake (UL) sand (sub-rounded) are used as test materials. Fig. 2 illustrates the particle size distribution, shape, and texture of sand materials used in the present study. A UB200i Lacet transmitting light microscope (integrated with DCM-900 digital camera) was used to capture the particle's shape. Therefore, different parts of the specimens were sampled randomly, and 50 grains were used. Particle shapes were determined, for a randomly picked subset of sand grains, using equations 1 to 2. Particle shape is described here in terms of sphericity and roundness. Sphericity (r_s) is a measure of convergence of particle's dimensions in the three-dimensional coordinate system. Particles with the highest sphericity contain minimum eccentricity and platiness. Roundness the (r_r) is a measure of surface features scale relative to the radius of the particle. Angular particles gain the minimum roundness index.

$$r_s = \frac{r_{max-in}}{r_{min-cir}} \tag{1}$$

$$r_r = \frac{\sum \frac{r_i}{N}}{r_{max-in}} \tag{2}$$

where, r_{max-in} is the equivalent particle radius or the radius of the largest sphere inscribing the particle, $r_{min-cir}$ is the radius of the smallest sphere circumscribing the particle, r_i is the equivalent average

radius of surficial features. The sphericity for F161, F131 and UL sands is 0.60, 0.68 and 0.85, respectively. The roundness for F161, F131 and UL sands is 0.38, 0.45 and 0.93, respectively. Table 1 summarizes the geometrical and physical properties of the three sands used for this study.

The diameter of the specimens for the triaxial tests, were 36mm and the height was 80mm. To achieve uniform density, specimens were prepared through dry pluviaition and by raining the dry mixture from a constant elevation through the air into the mould layer by layer. Dry air deposition was preferred to wet sedimentation in appreciation of the consequent hydration of fines and microstructural unwelcomed implications [17]. In this, specimens were remoulded to an initial natural open packing, similar to natural drift coastal deposits. Gaseous CO_2 and de-aired water were gently introduced through the bottom drainage, upwards through the specimen. Pore water pressure and cell pressure was then increased by the same increments to get the B-Skempton value to 0.96 which is deemed representative of soils' full saturated state. Saturated specimens were then isotopically consolidated to a range of initial confining pressures (i.e. initial effective mean principal stress, P'_c=100, 200, 300, and 400 kPa). Table 2 presents the list of tests educated for this study, quantifying each test specimen, the initial mean effective stress, void ratio after consolidation. Overall, 12 consolidated undrained (CU) shear tests were conducted on three sands (UL, F131, and F161 sands) for four levels of confining pressure (P'_c = 100, 200, 300 and 400 kPa). Drainage valves were closed and monotonic strain controlled undrained triaxial tests were conducted at 1mm/min strain rate.

Results and discussion

The steady States and Plastic Behaviour

Twelve undrained compression CU experiments were conducted on clean sand specimens. Figs. 3-5 (a-b) present the stress-strain and effective stress path data for all sand specimens. The data for F161 and F131

sands are plotted in Figs. 3-4, followed by the data for UL sand in Fig. 5. Pc' is the effective mean principal stress. USS is the Ultimate Steady State. The behaviour of sands appears to be almost independent of the effective mean principal stress (i.e. a change from 100 to 400 kPa), demonstrating a non-flow (NF) deformation where strain hardening (HS) occurs throughout undrained shearing to USS. Table 3 shows the different strength parameters of different types of sand.

Once the sand median grain size (D_{50}) increased and grain shapes scales ratios r_s and r_r decreased in the F131 sand, undrained shear strength, stress phase transformation point and ultimate steady state increased and soils behaviour move toward the dilative and strain hardening behaviour.

Phase transformation (PT) points of sands changed with medium grain size (D_{50}) and shape (r_r and r_s). Strengths of phase transformation (q_{pt}) increase with grain median grain size (D_{50}) and also increased with shape factors (r_r and r_s) reduction fig. 6. F 131 sand has the highest strength in PT point. Fig. 6 shows that q_{pt} increased with effective mean principal stress increment in all sand types.

Fig. 7 shows the effective mean principal stress in phase transformation point (p'_{pt}). P'_{pt} increased with D_{50} increment and shape factors (r_r and r_s) reduction. F131 sand has the highest effective mean principal stress in phase transformation point (p'_{pt}) and it shows that F131 had lower liquefiable potential. Also fig. 7 proposed that p'_{pt} increased with initial effective mean stress increment.

The peak strength of sands modified with medium grain size (D_{50}) and gran shape factors (r_r and r_s). Fig. 8 shows that the peak strength of F131 sand is highest due to highest D_{50} which is 0.91 mm. Peak strength (q_{peak}) increased with effective mean principal stress increment.

Ultimate steady state (USS) of sands diverse with size and shape factors. According to fig. 9 F161 sand has highest q_{uss}. It seems that F161 sand with low D_{50} and shape factors (r_r and r_s) respond stronger at the USS

(ageing and interlocking increment).The strength of USS (q_{uss}) increase with effective mean principal stress.

Strain Softening Indices

The observations on plastic volumetric behaviour of clean sands (presented in the previous section) necessitate the definition of a state index to quantify the softening i.e. flow potential. [29] suggested the use of u_f, the maximum excess pore water pressure ratio, as a measure of softening. The u_f index (i.e. herein known as flow potential) is controlled by stress conditions in the sand during both initial and shearing stages. Eq. 3 formulates the flow potential as a function of P'_{PT} (the mean effective pressure at the point of phase transformation) and P'_c (mean isotropic confining pressure).

$$u_f = 1 - \frac{P'_{PT}}{P'_c} \tag{3}$$

The variation of the flow index with effective mean principal stress (p'_c) is plotted in Fig. 10 for clean sand. For all confinement levels, relatively higher flow potential values were measured in UL sand: The flow potential appears to be directly proportional with D_{50} and (r_r and r_s) so pure sand specimens with lower angularity exhibit greater levels of flow potential. Flow potential is highest in 200 kPa confining pressure and then decreases with increase the confining pressure.

To better understand the relationship between the confining pressure and peak strength for clean sand, the dimensionless peak strength index (q_{peak}/P'_c) is here defined and quantified for test specimens – see Table 3. Fig 11 demonstrates the variation of the peak strength index with confining pressure for F161, F131 and UL sands. The peak strength generally decreases with increasing shape factors (r_r and r_s). Relatively greater orders of peak strength were achieved in F131 sand specimens for all levels of confining pressure. Peak strength is directly proportional with the confining pressure. Sandy samples with greater angularity offered greater orders of peak strength index.

Conclusions

From the series of undrained shear (CU) tests on three different sands with different particle sizes and morphological characteristics, the following major conclusions are drawn from the present work:

- Sands with a larger median grain size showed a greater dilative behaviour. Once the range of the sands' median grain size (D_{50}) increased while the grain shape scale ratios (r_r and r_s) diminished, the samples' strength, stress phase transformation point, and ultimate steady state were augmented and the behaviours shifted towards dilative and strain hardening.

- Phase transformation strength and peak strength is high in F131 sand with highest D_{50} and lowest shape factors in all confining pressures.

- USS points in all confining stress are high in f131 sand with lowest median grain size.

- The flow potential index decreased with increase the D_{50}, and improve with sand roundness in all confining stress. Flow potential index decreased with confining pressure increase. The peak strength index increased with D_{50} increment the host sands, diminished with shape factors increase, and grew in confining stress increase.

Reference

1. Kakou BG, Shimizu H, Nishimura S (2001) Residual strength of colluvium and stability analysis of farmland slope. Agric Eng Int CIGR J Sci Res Dev 3:1–12.

2. Petley DJ (1966) the shear strength of soils at large strains. PhD thesis, University of London.

3. Holtz WG, Gibbs HJ (1956) Triaxial shear tests on previous gravelly soils. J Soil Mech Found Div ASCE 820(SM1):1–22.

4. Patwardhan AS, Rao JS, Gaidhane RB (1970) Interlocking effects and shearing resistance of boulders and large size particles in a matrix of fines on the basis of large scale direct shear tests. In: Proc 2nd Southea Asian conf soil mech Singapore, pp 265–273.

5. Vallejo LE, Zhou Y (1994) The mechanical properties of simulated soil-rock mixtures. In: Proc 13th int'l conf soil mech and found engrg, New Delhi, pp 365–368.

6. Prakasha KS, Chandrasekaran VS (2005) Behavior of marine sand–clay mixtures under static and cyclic triaxial shear. J Geotech Geoenviron Eng 131(2):213–222.

7. Cho GC, Dodds J, Santamarina JC (2006) Particle shape effects on packing density, stiffness, and strength: natural and crushed sands. J Geotech Geoenviron Eng 132:591–602.

8. Simoni A, Houlsby GT (2006) The direct shear strength and dilatancy of sand–gravel mixtures. Geotech Geol Eng 24:523–549.

9. yama

10. Ghadr, S., and Assadi-Langroudi, A. 2018. Structure-based hydro-mechanical properties of sand-bentonite composites. Engineering Geology. 235, 53-63.

11. Tsomokos, A., and Georgiannou, V.N. 2010. Effect of grain shape and angularity on the undrained response of fine sands. Canadian Geotechnical Journal. 47, 539-551.

12. Oda, M., Koishikawa, I., and Higuchi, T. 1978. Experimental study of anisotropic shear strength of sand by plane strain tests. Soils and Foundations. 18(1), 25-38.

13. Dyskin AV, Estrin Y, Kanel-Belov AJ, Pasternak E (2001) Toughening by fragmentation—how topology helps. Adv Eng Mater 3(1):885–888.

14. Lim MS, Wijeyesekera DC, Zainorabidin A, Bakar I (2012) The effects of particle morphology (shape and sizes) characteristics on its engineering behaviour and sustainable engineering performance of sand. Int J Integr Eng 4:27–37.

15. Wadell H. 1932. Volume, shape, and roundness of rock particles. The Journal of Geology. 40(5), 443–451.

16. Hight DW, Georgiannou VN, Martin PL, Mundegar AK (1998) Flow slides in micaceous sand. In: Yanagisawa E, Moroto N, MitachiT (eds) Problematic soils. Sendai, Japan, pp 945–958.

17. Cubrinovski M, Ishihara K (2002) Maximum and minimum void ratio characteristics of sands. Soils Found 42(6):65–78.

18. Guimaraes M (2002) Crushed stone fines and ion removal from clay slurries—fundamental studies. Ph.D. thesis, Georgia Institute of Technology, Atlanta.

19. Santamarina, J.C., Cho, G.C., (2004) Soil behaviour: The role of particle shape. In: Proc. Skempton Conf. Advances in Geotechnical Engineering, Vol. 1, London, pp. 604–617.

20. Shahu, J.T., and Yudhbir. 1998. Model tests on sands with different angularity and mineralogy. Soils and Foundations, 38(4), 151-158.

21. Yagiz, S. 2001. Brief note on the influence of shape and percentage of gravel on the shear strength of sand and gravel mixtures. Bulletin of Engineering Geology and the Environment. 60(4), 321-323.

22. Nouguier-Lehon, C., Cambou, B., and Vincens, E. 2003. Influence of particle shape and angularity on the behaviour of granular materials: a numerical analysis. International Journal for Numerical and Analytical Methods in Geomechanics. 27(14): 1207-1226.

23. Kramer, S.L. and Seed, H.B. (1988) Initiation of Soil Liquefaction under Static Loading Conditions. Journal of Geotechnical Engineering, 114, 412-430.

24. Hight D.W., Bennell J.D., Chana B., Davis P.D., Jardine R.J. and Porovi_ E. 1997. Wave velocity and stiffness measurements of the Crag and Lower London Tertiaries at Sizewell. Geotechnique 47: 451-474.

25. Jefferies, M.G. & Been, K. 2006. Soil Liquefaction: A critical state approach, Taylor and Francis, Abingdon, ISBN.

26. Ishihara, K. "Liquefaction and Flow Failure During Earthquakes", 33rd Rankine Lecture, Gιotechnique 43, No. 3, 1993, pp 351-415

27. Lade, PV., and Ibsen, LB. 1997. A study of the phase transformation and the characteristic lines of sand behaviour. International Symposium on Deformation and Progressive Failure in Geomechanics, Nagoya, Japan.

28. Vaid, Y. P., Sivathayalan, S. (2000): "Fundamental factors affecting liquefaction susceptibility of sands," Canadian Geotechnical Journal, Vol. 37, pp. 592–606.

29. Yoshimine, M., Robertson, P.K. and Wride, C.E. 1999. Undrained shear strength of clean sands to trigger flow liquefaction. Canadian Geotechnical Joournal, 36: 891-906.

30. Yoshimine, M. and Ishihara, K. (1998). Flow potential of sands during liquefaction. Soils and Foundations, Vol. 38, No.3, pp. 189-198.

31. Yoshimine M, Ishihara K and Vargas W (1998) Flow deformation of sands subjected to principal stress rotation. Soils and Foundations 38(3): 179–188.

Table 1 Geometrical and physical properties of testing specimen constituents

Sand	F161	F131	UL
D_{10} : mm	0.16	0.65	0.085
D_{30} : mm	0.21	0.8	0.13
D_{50} : mm	0.27	0.91	0.15
D_{60} : mm	0.28	0.94	0.17
Cc	1.78	1.45	2.00
Cu	0.97	1.05	1.17
Gs	2.68	2.65	2.86
e_{min}	0.548	0.64	0.523
e_{max}	0.874	0.94	0.801
Fines content: FC:%	1	0	4

Table 2. Testing itinerary and specimens

No.	Soil name	P' (kPa)	e_c
1	F161	100	0.806
2	F161	200	0.784
3	F161	300	0.780
4	F161	400	0.775
5	F131	100	0.801
6	F131	200	0.781
7	F131	300	0.778
8	F131	400	0.771
9	UL	100	0.804
10	UL	200	0.785
11	UL	300	0.779
12	UL	400	0.774

Table 3. The investigated parameters of the reported tests

No.	Soil Type	p'_c(kPa)	q_{peak}(kPa)	q_{uss}(kPa)	q_{pt}(kPa)	p'_{pt}(kPa)	u_f
1	F161	100	46	203.6	63	77.3	0.227
2	F161	200	117.93	286.9	118.6	120.92	0.395
3	F161	300	213.14	519.64	218.6	218.79	0.271
4	F161	400	275.3	619.64	308.8	318.63	0.203
5	F131	100	72.8	195.56	84.63	90.83	0.092
6	F131	200	163.79	254.11	169.73	152.61	0.237
7	F131	300	265.59	413	286.95	258.6	0.138
8	F131	400	421.13	584.94	452.13	359.8	0.101
9	UL	100	40	197	59.98	61.92	0.381
10	UL	200	102	235	113.96	108.08	0.460
11	UL	300	192.9	391	213.49	200.53	0.332
12	UL	400	262	541	274.49	303.39	0.242
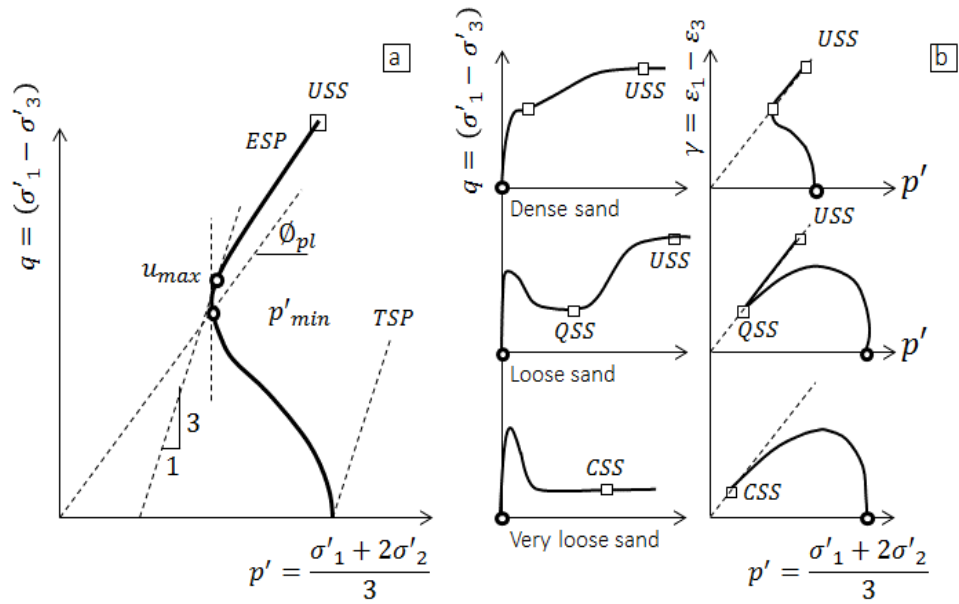
Figure 1. [a] Phase transformation state during undrained shearing of sand; [b] Steady states during undrained shearing of sand (After editorial adjustments − [31])
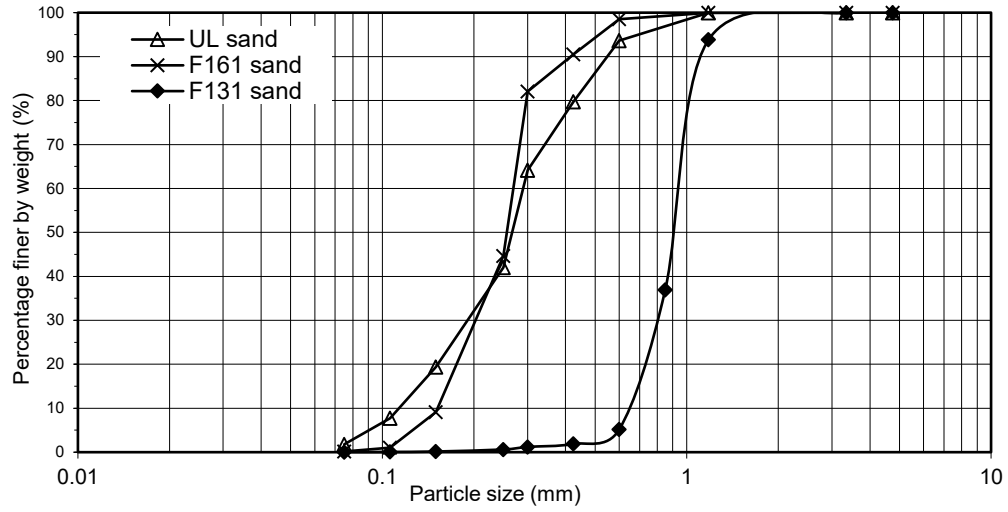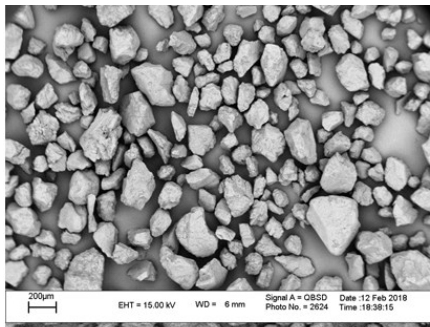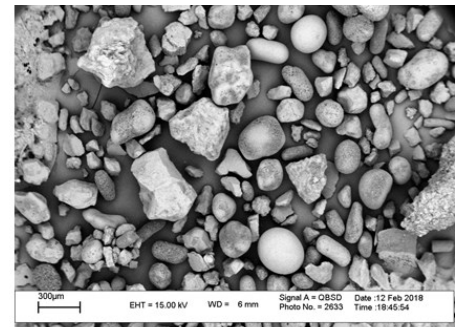
Figure 2. Particle size distribution, shape and texture of test specimen constituents (a) F131 (b) 161 (3) UL
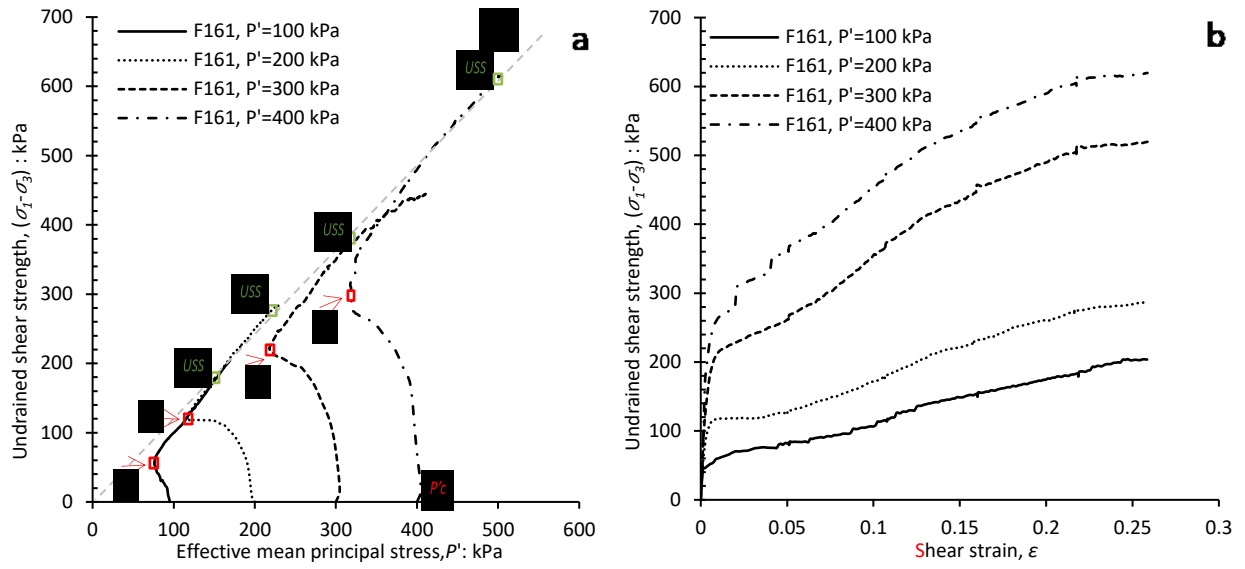
Figure 3. Undrained behaviour of F161 sand [a] Stress path on q-p' space; [b] stress-strain behaviour
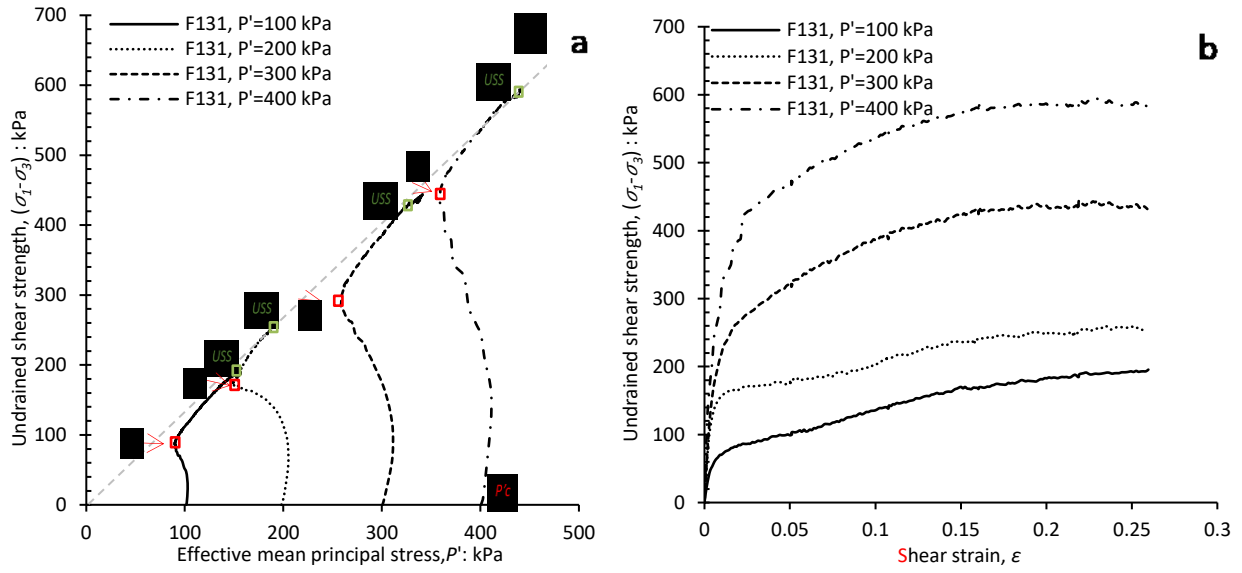
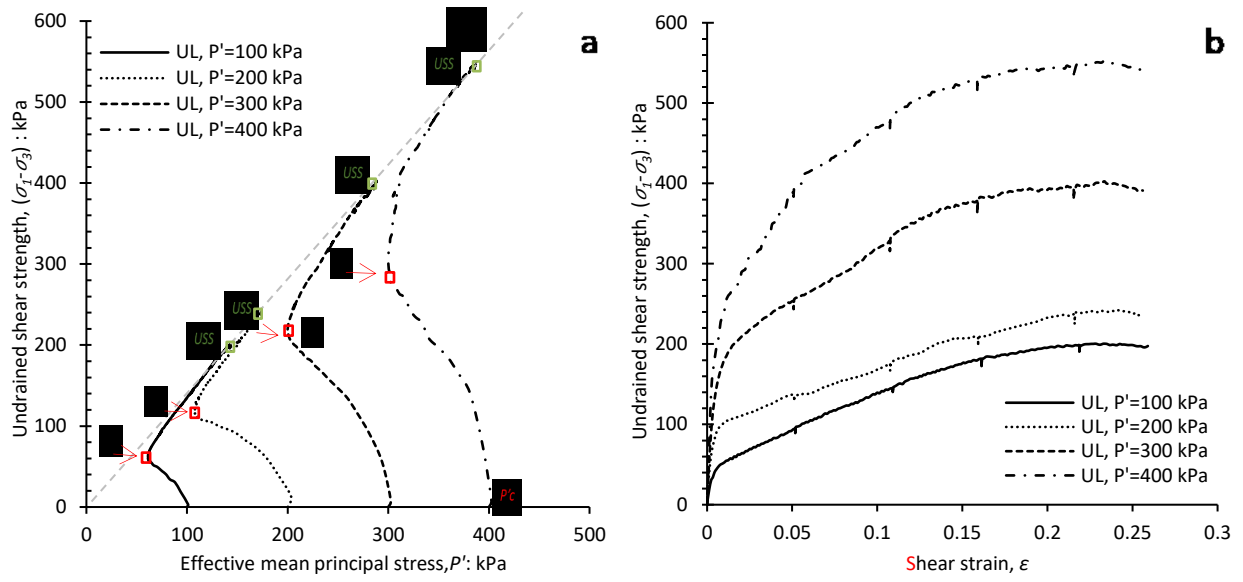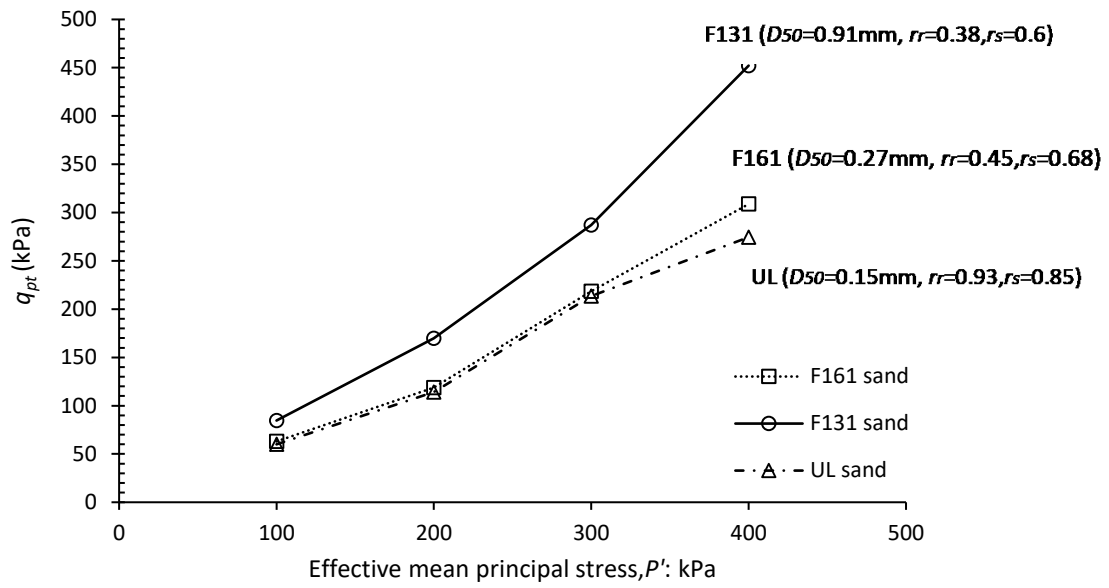Figure 4. Undrained behaviour of F131 sand [a] Stress path on q-p' space; [b] stress-strain behaviour

Figure 5. Undrained behaviour of UL sand [a] Stress path on q-p' space; [b] stress-strain behaviour

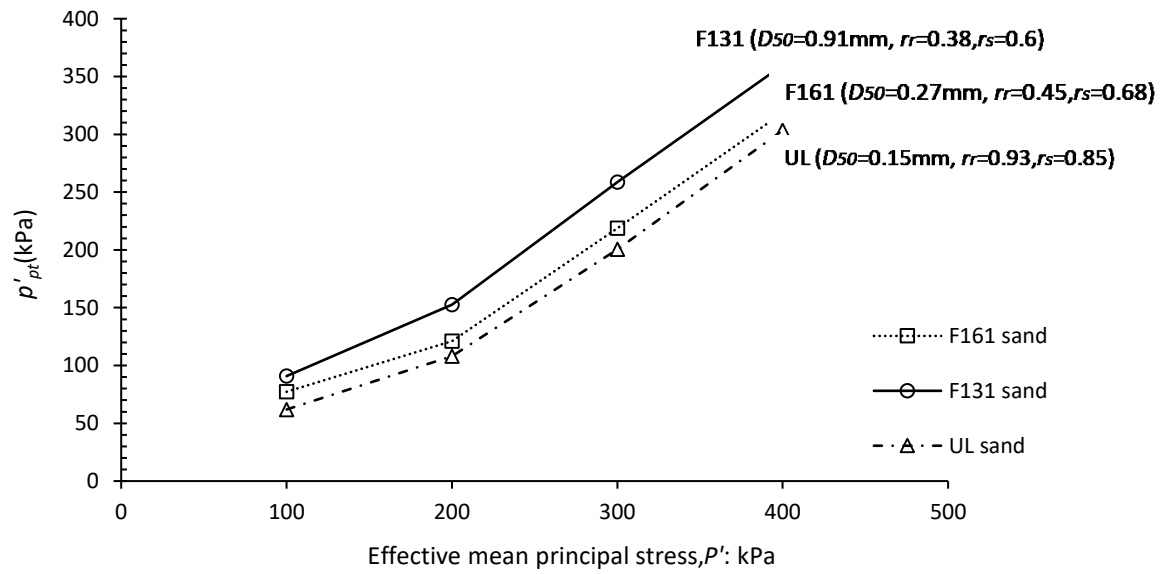20

Figure 6. Strength in phase transformation point of sands

Figure 7. Effective mean principal stress in phase transformation point of sands
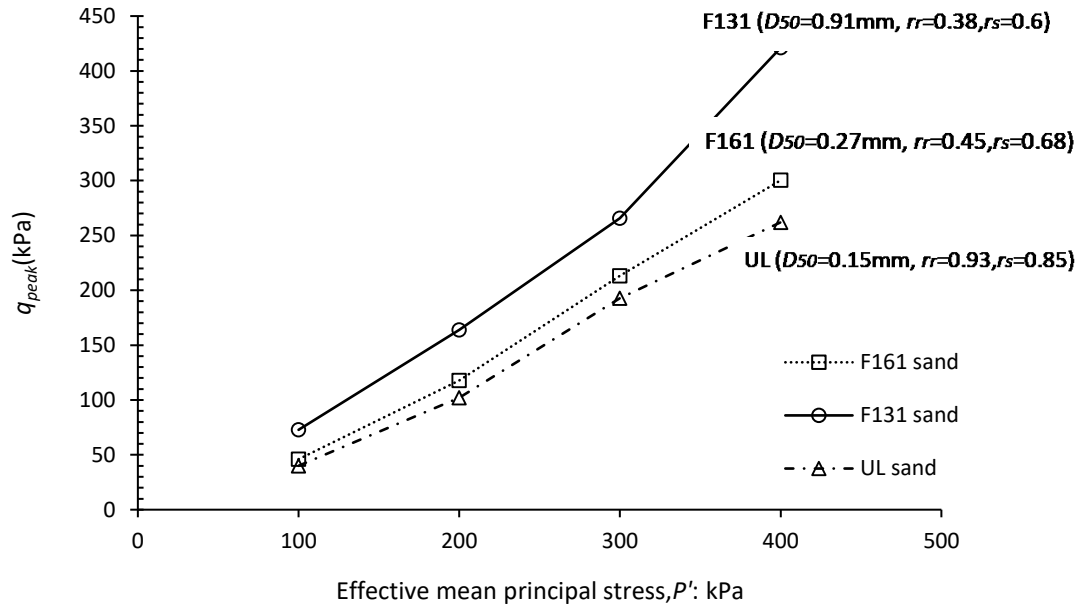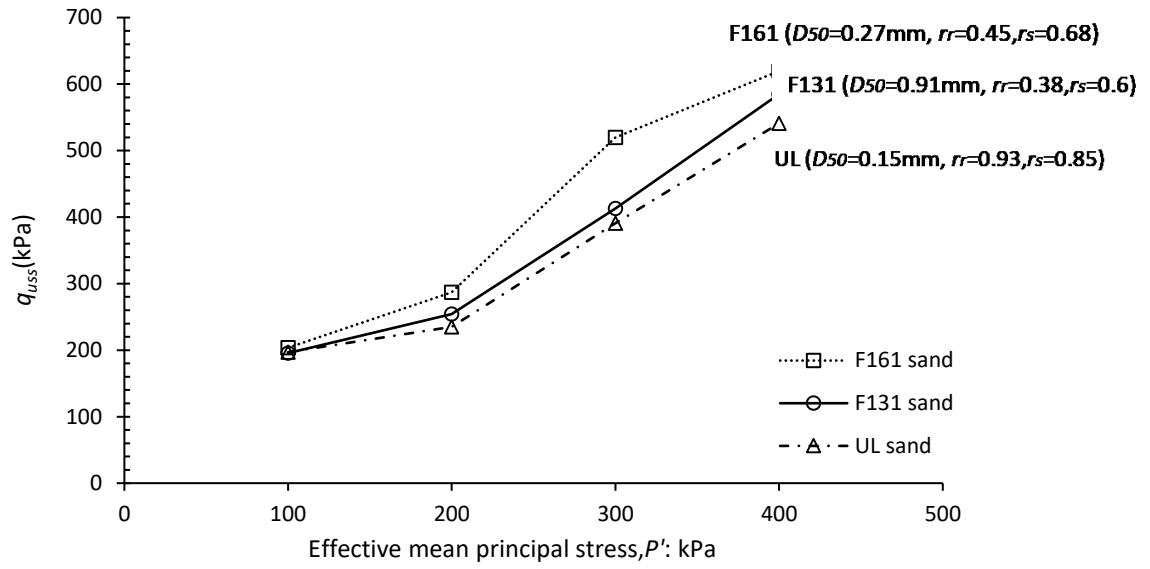
Figure 8. The peak strength of sands

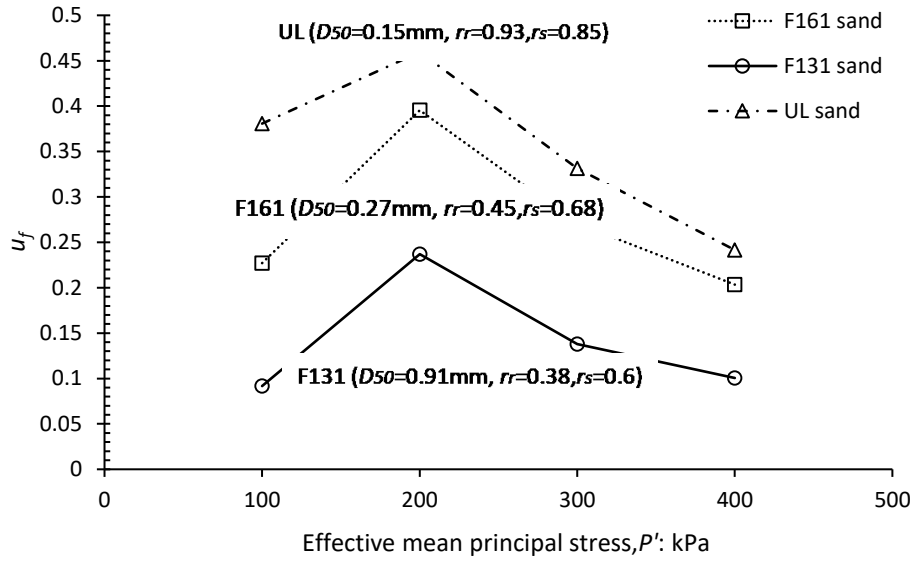Figure 9. Ultimate steady state (USS) modifications in sands

Figure 10. Demonstrates the variation of the flow potential index

F131 (*D50*=0.91mm, *rr*=0.38,*rs*=0.6)

F161 (*D50*=0.27mm, *rr*=0.45,*rs*=0.68)

UL (*D50*=0.15mm, *rr*=0.93,*rs*=0.85)

Peak index

Effective mean principal stress,*P'*: kPa
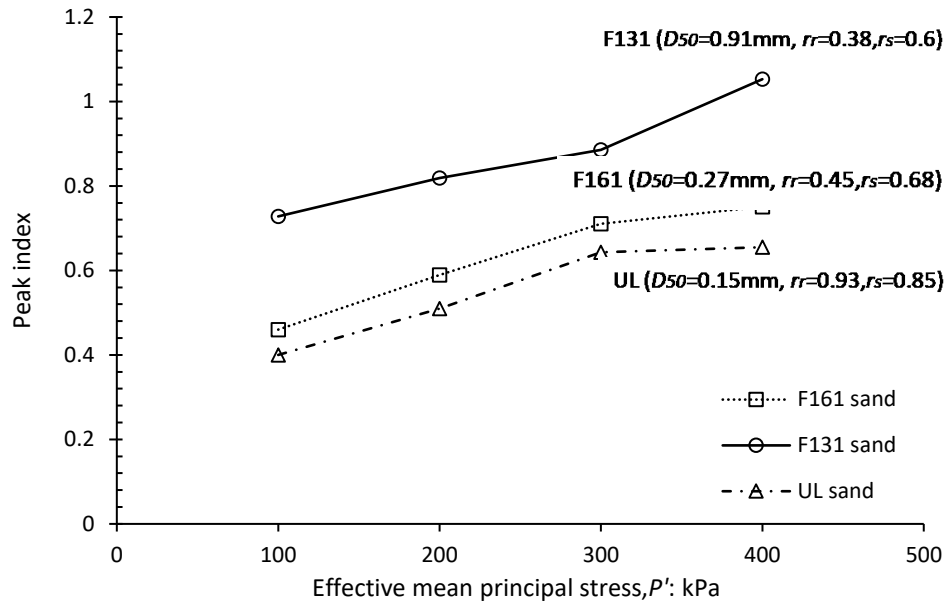
······□······ F161 sand

———○——— F131 sand

— · △ · — UL sand

Figure 11. Demonstrates the variation of the peak strength index